

THE ROLE OF STOCHASTIC RE-ACCELERATION IN THE PROMPT EMISSION OF GAMMA-RAY BURSTS:
APPLICATION TO HADRONIC INJECTION

KOHTA MURASE^{1,2}, KATSUAKI ASANO², TOSHIO TERASAWA^{2,3}, AND PETER MÉSZÁROS⁴

ABSTRACT

We study effects of particle re-acceleration in the post-shock region via magnetohydrodynamic/plasma turbulence, in the context of a mixed hadronic-leptonic model for the prompt emission of gamma-ray bursts (GRBs), using both analytical and numerical methods. We show that stochastically re-accelerated leptons, which are injected via pp and $p\gamma$ reactions and subsequent pair cascades, are able to reproduce the Band function spectra with $\alpha \sim 1$ and $\beta \sim 2-3$ in the \sim MeV range. An additional hard component coming from the proton-induced cascade emission is simultaneously expected, which is compatible with observed extra power-law spectra far above the MeV range. We also discuss the specific implications of hadronic models for ongoing high-energy neutrino observations.

Subject headings: gamma-ray burst: general — gamma rays: theory — radiation mechanisms: non-thermal

1. INTRODUCTION

The origin of prompt emission from gamma-ray bursts (GRBs) has been an open issue for more than 40 years. It is mainly observed in the $E \sim E^{\text{br}} \sim 10 \text{ keV} - 1 \text{ MeV}$ range, most spectra being fitted by a smoothed broken power-law (the so-called Band function) with break energy E^{br} . The typical low-energy photon index is $\alpha \sim 1$ (where $dF/dE \propto E^{-\alpha}$ below $\sim E^{\text{br}}$), while the typical high-energy photon index is $\beta \sim 2-3$ (where $dF/dE \propto E^{-\beta}$ above $\sim E^{\text{br}}$). Observed light curves are highly variable. The variability can sometimes be \sim ms, but pulses with various widths are observed. For typical long GRBs, light curves consist of many variable pulses, so that the duration, $T \sim 10^{1-2}$ s, is usually longer. So far, many models have been proposed to explain this most luminous phenomenon in our universe (see recent reviews, e.g., Mészáros 2006; Zhang 2007).

The classical scenario of the prompt emission is the optically-thin synchrotron internal shock model (e.g., Rees & Mészáros 1994), where shocks are responsible for dissipation of the outflow kinetic energy and observed gamma rays are attributed to synchrotron radiation from relativistic electrons. However, there are a couple of issues in the classical scenario. First, the low-energy photon index may be incompatible with values predicted by synchrotron emission (e.g., Ghisellini & Celotti 1999; Mészáros & Rees 2000). This is the case especially when relativistic electrons are in the fast-cooling regime, which leads to $\alpha \sim 1.5$, although the Klein-Nishina effect on synchrotron self-Compton (SSC) process may reproduce $\alpha \sim 1$ (e.g., Derishev et al. 2001; Wang et al. 2009; Daigne et al. 2011). One of the possible resolutions of this fast-cooling problem is to consider the magnetic field decay timescale that is comparable to the electron cooling timescale (Pe’er & Zhang 2006). Injection of electrons to acceleration processes is one of the related issues. Shock acceleration of primary electrons

may be inefficient for sufficiently small emission radii because of the rapid cooling in the strong magnetic field region at the vicinity of the shock (Medvedev & Spitkovsky 2009). If the outflow is magnetized enough, even for sub-luminal shocks, recent *ab initio* particle-in-cell simulations of collisionless shocks indicate that acceleration of nonthermal electrons at relativistic shocks are inefficient whereas ions can be accelerated (Sironi & Spitkovsky 2011). Another issue is the radiative efficiency problem (e.g., Ioka et al. 2006; Zhang et al. 2007), although this depends on estimates of the afterglow kinetic energy (Eichler & Waxman 2005). The high efficiency can be achieved by a large dispersion in the Lorentz factor of the outflows (e.g., Beloborodov 2000), but it does not seem so easy to reconcile that with the observed spectral correlations (e.g., Yonetoku et al. 2004). A recent discussion of the classical scenario is found in Daigne et al. (2011).

On the other hand, many alternative models have been suggested. Diffusive synchrotron radiation can explain the low-energy photon index if the fast-cooling problem is fixed (Medvedev 2000). Instead of dissipation of the kinetic energy via internal shocks, dissipation of the magnetic energy via, e.g., magnetic reconnection may play a crucial role as the dissipation mechanism, and observed gamma rays may be synchrotron or other electromagnetic radiation from relativistic electrons (e.g., Spruit et al. 2001; Lyutikov 2006; Zhang & Yan 2011; McKinney & Uzdensky 2011). If significant thermal energy is stored in the GRB jet by energy deposition from the central engine and/or via some dissipation below the photosphere, the prompt emission may originate from quasi-thermal emission caused by Comptonization or Coulomb heating (e.g., Thompson 1994; Ghisellini & Celotti 1999; Mészáros & Rees 2000; Pe’er et al. 2006; Ioka et al. 2007; Beloborodov 2010). One of the appealing possibilities is to consider the slow heating scenario. Around the photosphere, electrons that are slowly heated can lead to $\alpha \sim 1$ via Comptonization (Thompson 1994; Pe’er et al. 2006), where the typical electron energy is determined by the balance between heating and cooling (Ghisellini & Celotti 1999; Vurm & Poutanen 2009). Alternatively, in the neutron-rich outflow, Coulomb collisions should work as slow heating below the baryonic photosphere, leading to hard photon spectra of $\alpha \sim -0.5 - 1$ and $\beta \sim 2.5$ via the pair injection by the np reaction and

¹ Dept. of Physics; Center for Cosmology and AstroParticle Physics, Ohio State University, 191 West Woodruff Avenue, Columbus, OH 43210, USA

² Dept. of Physics, Tokyo Institute of Technology, 2-12-1 Ookayama, Meguro-ku, Tokyo 152-8550, Japan

³ Institute for Cosmic Ray Research, University of Tokyo, Kashiwa-no-ha 5-1-5, Kashiwa-shi, Chiba 277-8582, Japan

⁴ Dept. of Astronomy & Astrophysics; Dept. of Physics; Center for Particle Astrophysics, Pennsylvania State University, University Park, PA 16802, USA

subsequent cascades (Beloborodov 2010; Vurm et al. 2011). Such slow heating may be caused by stochastic acceleration (so-called second-order Fermi acceleration) over the sub-hydrodynamical timescale and/or hydrodynamical timescale, which may occur in the magnetohydrodynamic (MHD) and plasma turbulences generated by shock or magnetic dissipation such as magnetic reconnections (Bykov & Mészáros 1996; Asano & Terasawa 2009; Zhang & Yan 2011).

Emission at higher energies above ~ 10 MeV should also be important to reveal the radiation mechanism of the prompt emission, and various high-energy processes such as Comptonized thermal, SSC (Rees & Mészáros 1994; Asano & Inoue 2007), proton-induced cascade (Vietri 1997; Dermer & Atoyan 2006), and proton synchrotron (Totani 1998) emissions, were discussed. Such high-energy emission had been sparsely detected by the EGRET onboard the Compton Gamma-Ray Observatory (e.g., Hurley et al. 1994). Recently, however, significant observational progress has been achieved by *Fermi*. Dozens of GRBs have been observed by LAT onboard *Fermi*, and some bursts can be fitted by the Band function up to GeV energies (Abdo et al. 2009a; Abdo et al. 2009c; Abdo et al. 2010), while some of them (GRB 090510, 090902B, 090926A) clearly have an extra hard component at $\gtrsim 10$ MeV (Abdo et al. 2009b; Ackermann et al. 2010; Ackermann et al. 2011). GRBs with the extra GeV component belong to the brightest class of GRBs, which may indicate that this could be more common, even though it can be seen only in bright LAT GRBs (Granot 2010). Another feature found by *Fermi* is that $\gtrsim 100$ MeV gamma rays are delayed by $\sim 0.1 - 1$ s in the cosmological rest frame, behind the onset of the MeV emission.

The origin of the high-energy emission is now under active debate. Late-time high-energy gamma-ray emission from GRBs such as 080916C, 090510, and 090902B has been attributed to afterglow emission rather than the prompt emission (Kumar & Barniol Duran 2010; Ghisellini et al. 2010; Razzaque 2011). But, the high-energy emission in the early phase usually has a strong variability and often correlates with the MeV emission, which indicates an internal origin (He et al. 2011). Since the simple one-zone leptonic model often has difficulties, multi-zone models, not only the SSC model (Corsi et al. 2010; Daigne et al. 2011) but also the external inverse-Compton (IC) model (Toma et al. 2011; Pe’er et al. 2011) and the synchrotron model (Ioka 2010), have been invoked. The one-zone hadronic models are also viable, and the high-energy emission can be explained by proton-induced cascade or proton synchrotron emission (Asano et al. 2009b; Razzaque et al. 2010). The hadronic models are of interest, since GRBs may be the sources of observed ultra-high-energy cosmic rays (UHECRs), whose origin has been a big mystery for about 50 years (Waxman 1995; Vietri 1995; Murase et al. 2008), and their neutrino signals may be seen by ongoing neutrino observations (a recent review is Waxman 2011).

In this paper, we study a slow heating scenario in the presence of electromagnetic cascades initiated by injection at high energies. To explain the MeV emission self-consistently, we consider effects of re-acceleration of secondaries via the second-order Fermi mechanism, which can be anticipated in the post-shock region of relativistic shocks. We show that cascades can play an important role in the injection of re-accelerated particles, and slow heating scenarios via stochas-

tic acceleration typically lead to hard spectra compatible with observations. As an injection process at high energies, we consider an application to hadronic injection via pp and $p\gamma$ reactions, whereby the hadronic models have the appealing feature of explaining an extra hard component at GeV energies.

The paper is organized as follows. Section 2 describes an overview of the model, and we provide the numerical method and its results in Section 3. We discuss implications for neutrinos in Sections 4, and our results are summarized in Section 6. Throughout this work, cosmological parameters are set to $H_0 = 71$ km s $^{-1}$ Mpc $^{-1}$, $\Omega_M = 0.3$, and $\Omega_\Lambda = 0.7$, and we adopt the conventional notation $Q = Q_x \times 10^x$.

2. THEORETICAL MODEL

In this work, we investigate the role of particle re-acceleration, motivated by the goal to resolve the low-energy photon index and fast-cooling problems. In the post-shock region of relativistic shocks, turbulent magnetic fields would be generated, where stochastic acceleration (or second-Fermi acceleration) may work efficiently since the Alfvén velocity is close to c . The second-order Fermi acceleration over the sub-hydrodynamical scale plays a role of slow heating to avoid the fast cooling problem of relativistic electrons, and it may give harder electron spectra than the typical first-order Fermi acceleration. This possibility was proposed by Bykov & Mészáros (1996) and recently studied by Asano & Terasawa (2010).

Such slow heating operates not only for primary electrons but also electron-positron pairs generated via cascades initiated by some high-energy injection. Motivated by the electron injection/acceleration problem and the existence of an extra hard component at $\gtrsim 10$ MeV, this work focuses on a hadronic model, where pairs are produced via the electromagnetic cascade initiated by hadronic injection from $pp(np)$ and $p\gamma$ reactions, i.e., the proton-induced cascade. Although there is a similarity to the collisional scenario proposed by Beloborodov (2010), our scenarios are different in that leptons are heated by turbulence rather than Coulomb heating and the dissipation radius can be much larger.

The hadronic emission associated with prompt emission was originally motivated by the hypothesis that observed UHECRs come from GRBs (Waxman 1995; Vietri 1995; Murase et al. 2008). This requires that the UHECR energy (at $\sim 10^{19}$ eV) is comparable to the gamma-ray energy, $\tilde{\mathcal{E}}_{\text{HECR}} \equiv E_p'^2 (dN_p/dE_p') \sim \mathcal{E}_\gamma$. Although the GRB rate evolution, total gamma-ray energy and proton spectral index are still uncertain, the total nonthermal baryon loading is expected to be large, $\xi_{\text{CR}} \equiv \mathcal{E}_{\text{CR}}/\mathcal{E}_\gamma \sim 3 - 300$ (e.g., Murase et al. 2008; Waxman 2010, and references therein). If sufficiently large baryon loading is realized and the photomeson production efficiency is high enough, the hadronic emission can dominate over the leptonic emission at high energies (Asano et al. 2009a), and the visibility of the hadronic components at high energies is enhanced when the high-energy photon spectrum is much steeper than $\beta \sim 2$. The extra hard component in the GeV range, which was seen by *Fermi*, can be explained by the hadronic emission (Asano et al. 2009b). But, in the previous work, the Band function was assumed *ad hoc*, otherwise the low-energy photon index becomes too soft (which also leads to overestimating gamma rays and neutrinos).

In the next subsection, we consider shock dissipation in the

baryonic outflow and shock acceleration of particles. Then, we discuss stochastic particle acceleration by plasma/MHD turbulence in the downstream region to take into account its effects phenomenologically with a simplified model.

2.1. Shock Acceleration at Internal Shocks

In the classical scenario, electrons are accelerated at internal shocks, and the observed gamma-ray emission is attributed to electromagnetic radiation from non-thermal electrons. If the outflow contains baryons, it is natural to expect that protons are also accelerated on a timescale

$$t_{\text{acc}} = \eta \frac{rL}{c}, \quad (1)$$

where $\eta \sim 1 - 10$ in the efficient case (e.g., Bednarz & Ostrowski 1996; Rachen & Mészáros 1998). The acceleration timescale is typically fast, and protons that are accelerated up to sufficiently high energies should interact with non-thermal photons via photomeson production, leading to \sim PeV neutrinos (Waxman & Bahcall 1997; Rachen & Mészáros 1998), GeV-TeV gamma rays (Vietri 1997), and UHE gamma rays (Murase 2009). Around the photosphere, GeV-TeV neutrinos and GeV-TeV gamma rays are also produced through the $pp(np)$ reaction (Murase 2008; Wang & Dai 2009).

In our model, we consider a similar picture in which charged particles are accelerated at shocks. Motivated by the electron injection/acceleration issue, however, we focus on the case of hadronic injection (neglecting primary electrons), where proton-induced gamma-ray emission is especially relevant. When the shock dissipation radius is small enough, the efficient $pp(np)$ reaction occurs in the baryon-rich outflow, and high-energy gamma rays and pairs are produced as well as neutrinos. Also, sufficiently high-energy protons can interact with soft photons which may come from residual thermal emission around the photosphere (Asano & Takahara 2003) (and/or non-thermal emission from primary electrons if their acceleration occurs). Those pp and $p\gamma$ reactions lead to production of high-energy gamma rays with $E \sim 0.1E_p \simeq$ TeV $E_{p,12}$ and pairs with $E_e \sim 0.05E_p \simeq 0.5$ TeV $E_{p,12}$. Lower-energy photons should also be produced via the synchrotron and IC processes, which eventually affect the distribution of seed photons so that the processes are nonlinear.

Sufficiently high-energy gamma rays should lead to pair creation with seed photons at $\tilde{E}E \approx \Gamma^2 m_e^2 c^4$, so that the following cascade is unavoidable. As long as the pair-creation opacity of high-energy gamma rays is larger than unity, gamma rays lead to generation of pairs that lose their energies via synchrotron and IC emissions. As a result, the cascade gamma-ray spectrum will be eventually formed, where the number of pairs can be larger than that of pairs injected directly from the pp and $p\gamma$ reactions.

We are interested in cases where the pp or $p\gamma$ reaction efficiency is high enough, otherwise the hadronic component is insufficient to explain the high-energy gamma-ray emission observed by *Fermi*. Hence, for the demonstrative purpose, this work focuses on relatively small dissipation radii of $r \sim 10^{12-13}$ cm such that $\tau_T \approx \sigma_T n_{\text{th}} l \sim 0.1 - 1$ (where n_{th} is the thermal proton density and l is the co-moving length), though large uncertainty allows us to consider different cases where the pp and $p\gamma$ reaction efficiencies are much lower (e.g., Murase et al. 2008). The pp reaction efficiency is roughly estimated to be $f_{pp} \approx \kappa_{pp} \sigma_{pp} n_{\text{th}} l \simeq 0.05 \tau_T$ (Murase 2008), where κ_{pp} is the pp inelasticity of

protons. We expect that the observed gamma-ray spectrum will be eventually formed (see the next section). Then, assuming the (broken) power-law photon spectrum, the effective photomeson production efficiency is estimated to be (Waxman & Bahcall 1997; Murase & Nagataki 2006b)

$$f_{p\gamma}(E_p) \sim 0.7 \frac{L_{\gamma,51.5}^{\text{br}}}{r_{13} \Gamma_{2.7}^2 (E^{\text{br}}/500 \text{ keV})} \begin{cases} (E_p/E_p^{\text{br}})^{\beta-1} & (E_p < E_p^{\text{br}}) \\ (E_p/E_p^{\text{br}})^{\alpha-1} & (E_p^{\text{br}} < E_p) \end{cases}. \quad (2)$$

where $E_p^{\text{br}} \simeq 80$ PeV $(E^{\text{br}}/500 \text{ keV})^{-1} \Gamma_{2.7}^2$ is the energy of protons interact with photons with E^{br} and the multi-pion production effect is included.

Gamma rays also interact with the same target photon field, so that the above equation implies that the pair-creation opacity is (e.g., Lithwick & Sari 2001; Gupta & Zhang 2008)

$$\begin{aligned} \tau_{\gamma\gamma}(E) &\approx \frac{f(\beta) \sigma_T l L_{\gamma}^{\text{br}}}{4\pi r^2 \Gamma c E^{\text{br}}} \left(\frac{E E^{\text{br}}}{\Gamma^2 m_e^2 c^4} \right)^{\beta-1} \\ &\sim 280 \frac{L_{\gamma,51.5}^{\text{br}}}{r_{13} \Gamma_{2.7}^2 (E^{\text{br}}/500 \text{ keV})} \begin{cases} (E/\tilde{E}^{\text{br}})^{\beta-1} & (E < \tilde{E}^{\text{br}}) \\ (E/\tilde{E}^{\text{br}})^{\alpha-1} & (\tilde{E}^{\text{br}} < E) \end{cases} \end{aligned} \quad (3)$$

where $\tilde{E}^{\text{br}} \simeq 130$ GeV $(E^{\text{br}}/500 \text{ keV})^{-1} \Gamma_{2.7}^2$ and $f(\beta) \sim 0.1$ for $\beta \sim 2$ (Baring 2006). (Note that the opacity in the highest energies can be smaller than unity due to existence of the synchrotron self-absorption cutoff.) Then, in a simple one-zone model, the pair-creation break (or cutoff) is estimated to be $E^{\text{cut}} \simeq 1.3$ GeV $(L_{\gamma,51.5}^{\text{br}})^{-\frac{1}{\beta-1}} r_{13}^{\frac{1}{\beta-1}} \Gamma_{2.7}^{\frac{2\beta}{\beta-1}} (E^{\text{br}}/500 \text{ keV})^{\frac{2\beta}{\beta-1}}$. Most of the high-energy gamma rays are radiated below this energy, and the above equation suggests that the effective injection rate of pairs is

$$Q_i \sim \frac{\min[1, \langle f_{\text{mes}} \rangle] U_p G_{\varepsilon}}{t_{\text{dyn}}}, \quad (4)$$

where U_p is the total cosmic-ray proton energy density, $t_{\text{dyn}} \approx 3l/c$ is the dynamical time scale, $\langle f_{\text{mes}} \rangle$ is the effective meson production efficiency averaged over proton energies, and G_{ε} such that $\int d\varepsilon G_{\varepsilon} = 1$ is determined by the details of the cascade. Because of the pair cascade and the multiplicity of the hadronic reactions, the number of electron-positron pairs can be even larger than that of the reactions (cf. Beloborodov 2010). If there is no re-acceleration and escape, we have

$$\frac{\partial n_{\varepsilon}}{\partial t} = \frac{\partial}{\partial \varepsilon} \left[\frac{d\varepsilon}{dt} n_{\varepsilon} \right] + Q_i, \quad (5)$$

where

$$\frac{d\varepsilon}{dt} = -\frac{4}{3} \sigma_T c (U_B + U_{\text{KN}}) (\gamma^2 - 1) \quad (6)$$

and U_B is the magnetic field energy density and U_{KN} is the photon energy density with the correction by the Klein-Nishina effect. Therefore, at energies where injection occurs, we expect that the cascade typically leads to a flat energy spectrum of electrons, so that we obtain $EF(E) \propto E^{-0.5}$ that is also seen by our numerical calculations. Such hard photon spectra can explain the extra hard component at $\gtrsim 10$ MeV observed by *Fermi* (e.g., Asano et al. 2009b). In the hadronic model that attributes the extra high-energy component to the proton-induced cascade, one typically expects

$$\mathcal{E}_{\gamma\text{ex}} \sim \min[1, \langle f_{\text{mes}} \rangle] \mathcal{E}_{\text{CR}}, \quad (7)$$

where $\mathcal{E}_{\gamma\text{ex}}$ is the energy in gamma-rays of the extra component, which is typically smaller than the total gamma-ray energy released as prompt emission, \mathcal{E}_{γ} . As the emission radius is larger (leading to lower $\langle f_{\text{mes}} \rangle$), larger \mathcal{E}_{CR} is required.

2.2. Stochastic Acceleration in Turbulence

Next, we consider stochastic acceleration of particles that are produced by injection at high energies and subsequent cascades. The turbulent magnetic field in the downstream of the shock is expected to be significantly amplified. Cascade pairs that are rapidly cooling (i.e., they are in the fast cooling regime) are distributed in the downstream region, and can be re-accelerated by plasma/MHD turbulence via the second-order Fermi mechanism. Assuming isotropy of the particle momenta and of the fluctuations, one may apply the Fokker-Planck equation (e.g., Liu et al. 2006; Brunetti & Lazarian 2007),

$$\frac{\partial n_\varepsilon}{\partial t} = \frac{\partial}{\partial \varepsilon} \left(D_{\varepsilon\varepsilon} \frac{\partial n_\varepsilon}{\partial \varepsilon} \right) - \frac{\partial}{\partial \varepsilon} \left[\left(A - \frac{d\varepsilon}{dt} \right) n_\varepsilon \right] - \frac{n_\varepsilon}{t_{\text{esc}}} + Q_i, \quad (8)$$

where $A = (D_{\varepsilon\varepsilon}/\varepsilon)(1 - \gamma^{-2})/(1 + \gamma^{-1})$ and $D_{\varepsilon\varepsilon}$ is the diffusion coefficient. For a broad range of the isotropic magnetic field fluctuations with spectral energy density $W_k \propto k^{-q}$, we expect $D_{\varepsilon\varepsilon} \propto \varepsilon^q$ for resonant acceleration, where scattering and acceleration timescales of charged particles are proportional to $\varepsilon^2/D_{\varepsilon\varepsilon} \propto \varepsilon^{2-q}$ (e.g., Miller & Ramaty 1989; Dermer et al. 1996). For non-resonant acceleration, one may expect $D_{\varepsilon\varepsilon} \propto \varepsilon^2$ (Brunetti & Lazarian 2007). The fluid and particles behind the shock are advected to the downstream so that the length scale of the turbulent region will be $l_{\text{tur}} \approx (c/3)t_{\text{tur}}$, where t_{tur} is the typical lifetime of the turbulence. Then, since the Alfvén velocity is expected to be $\sim c$, for fluctuations with a simple power law, the stochastic acceleration timescale is expressed as (Dermer et al. 1996; Bykov & Mészáros 1996; Petrosian & Liu 2004)

$$t_{\text{sta}} \equiv \frac{\varepsilon^2}{4D_{\varepsilon\varepsilon}} = \eta_{\text{sta}} \frac{l_{\text{tur}}}{c} \left(\frac{r_L}{l_{\text{tur}}} \right)^{2-q}, \quad (9)$$

where r_L is the Larmor radius, $\eta_{\text{sta}} \sim 1$ is a pre-factor, and we have assumed that $2\pi/k_{\text{min}} \sim l_{\text{tur}}$. This stochastic acceleration timescale can be longer than the shock acceleration timescale, $t_{\text{acc}} = \eta r_L/c$. But it can still be shorter than the hydrodynamical timescale, l_{tur}/c , in the relevant energy range where $r_L \ll l_{\text{tur}}$ (except for exactly $q = 2$ over all k). In this sense, the stochastic acceleration plays the role of a slow heating over the sub-hydrodynamical timescale (Bykov & Mészáros 1996).

Various numerical simulations have recently been attempted (e.g., Chang et al. 2008; Zhang et al. 2009; Mizuno et al. 2011; Inoue et al. 2011). Generally speaking, the turbulent spectrum may not be a simple power law and q may be rather k -dependent, and the MHD simulations have suggested the spectrum is flat at large scales but quite steep at small scales above the transition scale. At present, however, we still have no complete model of relativistic turbulence for GRB internal shocks. Hence, as in previous work (Asano & Terasawa 2009), we consider the simplest case where the stochastic acceleration time is energy-independent in the range in which we are interested. Since $r_L \ll l_{\text{tur}}$ for relevant electron energies and sufficiently steep turbulent spectra can be expected at small scales (e.g., Chang et al. 2008; Inoue et al. 2011), stochastic acceleration can be effectively non-resonant. Although future numerical studies on plasma/MHD turbulence are required for more realistic calculations, our phenomenological approach is enough to demonstrate the role of stochastic acceleration and it would be approximately valid in the relatively narrow energy range relevant for the MeV emission.

Next, we briefly discuss the expected spectra of particles reaccelerated via stochastic acceleration, although the details depend on diffusion, energy losses, and particle escape. Let us consider low energies where energy losses are negligible. Then, for $q = 2$, the steady-state spectrum is obtained as $n_\varepsilon \propto \varepsilon^{0.5 - (9/4 + 4t_{\text{sta}}/t_{\text{esc}})^{1/2}}$ (Liu et al. 2006). At sufficiently low energies ($r_L \ll l_{\text{tur}}$) that are relevant in the case of GRB prompt emission, t_{esc} is so long that we may drop it, where one has $n_\varepsilon \propto \varepsilon^{1-q}$. This means that the stochastic acceleration leads to hard electron spectra, and the energy spectrum of synchrotron photons is expected to be

$$EF(E) \propto E^{2-q/2}, \quad (10)$$

for $q > 4/3$. Hence, the low-energy photon index of $\alpha \sim q/2 \sim 1$ is possible if $q \sim 1.5 - 2$. In the classical scenario of prompt emission, electrons are typically in the fast cooling regime, so that high-energy electrons cool down within the advection time, $\sim 3l/c$. But, this problem can be avoided when acceleration plays a role of slow heating.

When cooling is absent, the maximum energy of re-accelerated electrons should eventually be limited, since they can carry only a fraction of the turbulent energy. Or, radiative cooling is so strong that the typical electron energy is determined by the balance between acceleration and cooling. If we knew the turbulent spectrum from first principles, we would be able to calculate γ_{typ} . For example, if the turbulent spectrum is flat at large scales and then becomes sufficiently steep at $\sim 100k_{\text{min}}$, the stochastic acceleration time can be $t_{\text{sta}} \sim 1.3 \times 10^{-5}$ s ($l_{\text{tur}}/0.2l$) $r_{13} \Gamma_{2.7}^{-1}$. Comparison with the synchrotron cooling time of $t_{\text{syn}} \simeq 1.8 \times 10^{-5}$ s $\epsilon_{B,-1}^{-1} r_{13}^2 \Gamma_{2.7}^2 L_{\text{th},53.5}^{-1} \gamma_{2.7}^{-1}$ (where ϵ_B is the energy fraction carried by magnetic fields and L_{th} is the luminosity associated with the thermal energy) gives $\gamma_{\text{typ}} \sim 690 \epsilon_{B,-1}^{-1} (l_{\text{tur}}/0.2l)^{-1} r_{13} \Gamma_{2.7}^3 L_{\text{th},53.5}^{-1}$ leading to \sim MeV synchrotron gamma rays. Unfortunately, however, the realistic stochastic acceleration rate is highly uncertain at present so that we instead make an *ad hoc* assumption that the stochastic acceleration rate is determined by requiring that the observed break energy is the synchrotron energy of electrons with the typical electron Lorentz factor (Asano & Terasawa 2009), where we find⁵

$$\begin{aligned} \gamma_{\text{typ}} &\approx \left(\frac{E^b m_e c}{\Gamma h e B} \right)^{1/2} \\ &\simeq 550 r_{13}^{1/2} \epsilon_{B,-1}^{-1/4} \left(\frac{E^b}{500 \text{ keV}} \right)^{1/2} L_{\text{th},53.5}^{-1/2}. \end{aligned} \quad (11)$$

As described in the next section, we take into account stochastic acceleration of leptons by using the Monte Carlo method, assuming that the acceleration time is energy-independent and equation (11) applies. Although it is a toy model, we can demonstrate that the re-accelerated particles have hard spectra leading to $\alpha \sim 1$, as expected in this subsection.

⁵ Phenomenologically, one can obtain another expression, $\gamma_{\text{typ}} \sim \left[\frac{3-q}{2-q} \frac{\epsilon_e}{f_e} \frac{m_p}{m_e} \gamma_{p,\text{th}} \frac{1-q}{\gamma_{\text{reacc}}} \right]^{1/(2-q)}$ for $q < 2$ or $\gamma_{\text{typ}} \sim \ln \left(\frac{\gamma_{\text{typ}}}{\gamma_{\text{reacc}}} \right) \frac{\epsilon_e}{f_e} \frac{m_p}{m_e} \gamma_{p,\text{th}}$ for $q \sim 2$. Here ϵ_e is the energy fraction carried by electrons accelerated via turbulence and γ_{reacc} is the electron Lorentz factor at which the stochastic acceleration does not operate (which can be expected when particles do not interact with plasma/MHD waves). Then, f_e is the effective number fraction of electrons that are injected to the stochastic acceleration, which is determined by the details of the cascade and acceleration processes.

3. NUMERICAL RESULTS OF GAMMA-RAY SPECTRA

In the previous section, we gave the basic picture of our model with analytical expressions. But many microphysical processes have to be taken into account in order to calculate gamma-ray spectra. One of the approaches is to solve the kinetic equations (e.g., Svensson 1987), but it is time consuming for our problem. Alternatively, we employ the Monte Carlo code used in, e.g., Asano et al. (2009a), Asano & Terasawa (2009), where the energy distributions of all particles are simulated iteratively until they converge to a self-consistent steady state, which is assumed to be realized within the pulse timescale.

All the important microphysical processes for the electromagnetic cascade, $\gamma\gamma$ pair creation by electron and positron pairs, synchrotron, and Compton (both in the Thomson and Klein-Nishina regimes) emissions from all relativistic particles, and synchrotron self-absorption, are properly included (e.g., Blumenthal & Gould 1970). The photomeson production is approximately included as in Asano & Nagataki (2006), using experimental data but neglecting high-multiplicity/inelasticity, multi-pion production at high energies, and it is assumed that a muon neutrino from pion decay carries a quarter of the pion energy, and neutrinos and a lepton from muon decay carry a third of of the muon energy. Note that such a simplified treatment is timesaving and sufficient for this work, since effects of more detailed microphysics are typically moderate (Murase & Nagataki 2006a; Murase 2007; Baerwald et al. 2011). The Bethe-Heitler process by protons is also included using the cross section and inelasticity given by Chodorowski et al. (1992), but this effect is only modest in the relevant energy range for GRB prompt emission spectra (e.g., Mannheim et al. 2000). In addition, we implement in detail the pp reaction for which high multiplicity and inelasticity in pion production is important. The high-energy process is calculated as in Murase (2008), whereas the low-energy process below 100 GeV is included based on runs of Geant 4 (Agostinelli et al. 2003). The Thomson scattering effect due to thermal electrons, which would weaken photons of energy above $\sim m_e c^2$ in the comoving frame, is included by assuming that photons interact with electrons of temperature 100 keV within a timescale l/c before they escape from the emission region. The spectral softening by this effect has been calculated with a Monte-Carlo method with the Klein-Nishina cross section calculated in advance.

There are several input parameters required for calculations. The emission radius r and the bulk Lorentz factor Γ are relevant parameters. One typically expects $r \sim 10^{13} - 10^{15.5}$ cm in the classical internal shock scenario, or $r \sim 10^{11} - 10^{13}$ cm in the baryonic photospheric scenario. We consider relatively small radii (but larger than the coasting radius), $r \sim 10^{12} - 10^{13}$ cm, where the efficient hadronic reactions are efficient (Asano 2005; Murase & Nagataki 2006a). We also take $\Gamma \sim 100 - 1000$, and the comoving length is given by $l = r/\Gamma$. Another important parameter is the luminosity of protons accelerated at the shock, $L_p = 4\pi r^2 \Gamma^2 c U_p$ (and the nonthermal baryon loading parameter is expressed as $\xi_{\text{CR}} = L_p/L_\gamma$). In this work, we consider $L_p \sim 10^{53} - 10^{54}$ erg s $^{-1}$, assuming the proton distribution with $dn_p/d\varepsilon \propto \varepsilon_p^{-2} e^{-(\varepsilon_p/\varepsilon_p^{\text{max}})}$ for $\varepsilon_p \geq \gamma_{\text{th}} m_p c^2 = 4m_p c^2$. The maximum energy $\varepsilon_p^{\text{max}}$ is given by the comparison between the acceleration time and cooling timescales as well as the Hillas condition. We also assume the luminosity associated with the thermal energy,

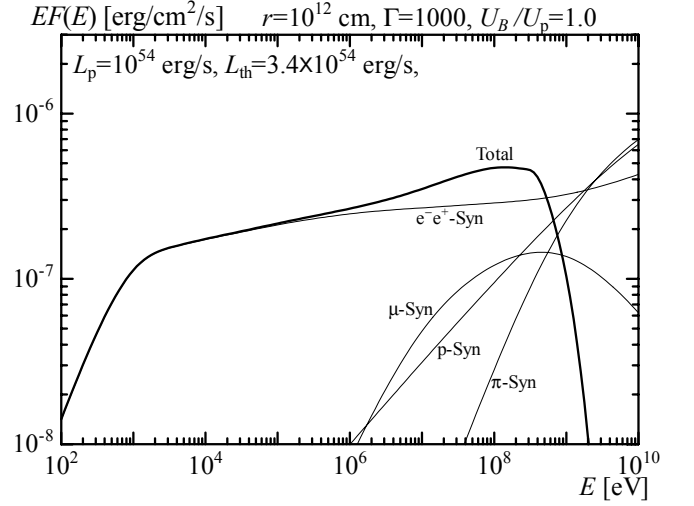


FIG. 1.— Gamma-ray spectra of proton-induced cascade emission without stochastic re-acceleration. The source redshift is assumed to be $z = 1$. The strong magnetic field is assumed over the length scale of $l_{\text{tur}} = 0.17l$ and $\eta = 1$ is assumed. The corresponding Thomson depth is $\tau_T = 1$.

$L_{\text{th}} = 4\pi r^2 \Gamma^2 c U_{\text{th}} (\gtrsim L_p)$, where $U_{\text{th}} = \gamma_{\text{th}} n_{\text{th}} m_p c^2$ is the thermal energy density. The comoving magnetic field is introduced as $U_B (= \varepsilon_B U_{\text{th}}) \sim 0.01 - 1 U_p$. In accord with our motivation and purposes, we neglect the acceleration of primary electrons.

In Figure 1, we show an example of the proton-induced cascade emission. The $p\gamma$ and pp reactions lead to very high-energy gamma rays which eventually cascade down via pair creation, synchrotron and Compton emissions. (Note that we include both IC scattering and Compton downscattering.) The proton synchrotron component also contributes to the intrinsic very high-energy component but it is significantly attenuated and cascaded in the source. Then, as expected before, a flat and hard spectrum, which is different from the Band function, is typically obtained below the pair-creation cutoff. Note that such a flat and hard spectrum is expected for larger dissipation radii as studied in detail by Asano et al. (2009a).

Now, we take into account effects of stochastic acceleration. We give the energy gain/loss per collision, $\Delta\varepsilon/\varepsilon$, following the Gaussian probability function, according to Asano & Terasawa (2009) that focused on the case of low-energy injection where the cascade does not play an important role. Then, we set the stochastic acceleration rate such that the synchrotron peak of γ_{typ} electrons correspond to E^{br} . We also introduce sub-parameters, γ_{reacc} and l_{tur} , but our main results are not sensitive to those additional parameters. The former is related to how long stochastic acceleration operates, and $\gamma_{\text{reacc}} \ll \gamma_{\text{typ}}$ is needed for the re-acceleration to work well. Since the calculations for $\gamma_{\text{reacc}} \sim 1$ are too time-consuming, we take $\gamma_{\text{reacc}} \sim 10 - 100$, which is enough for our purpose. The latter parameter is physically motivated by the finite lifetime of the turbulent magnetic field, and we assume $l_{\text{tur}}/l \sim 0.1 - 1$ in this work. Thus, our “one-zone” code divides the shocked region into two parts: a strongly magnetized region of scale l_{tur} and the second, remaining part of scale $l - l_{\text{tur}}$. The photon density is assumed to be homogeneous over the entire scale l , and secondary particles from protons would be injected also homogeneously in this scale. But, for simplicity, we treat only a fraction l_{tur}/l of the secondary particles injected in the strongly magnetized region. Although IC emission by the particles injected in the non-disturbed region may

appear in the GeV range (Asano & Terasawa 2009), we neglect such emission. The absence of heating in this region may make such emission less important. The parameter l_{tur} can affect high-energy IC spectra quantitatively, but the qualitative features of our results are not altered (see below). The calculation time is set to $t_{\text{tur}} = 3l_{\text{tur}}/c$ for the secondary particles, while that for accelerated protons is l/c . We do not consider stochastic acceleration of protons since more efficient shock acceleration is assumed. We also remark that the energy ranges for pion-producing protons and electrons with $\sim \gamma_{\text{typ}}$ are quite different. Also, we neglect re-acceleration of pions and muons, though it might be potentially relevant (see appendix A).

In Figure 2, we show the case where stochastic re-acceleration is included, for the same parameter set shown in Figure 1. When the re-acceleration is turned on, electrons and positrons can avoid their fast cooling, and the energy balance between acceleration and cooling gives the typical energy of $\gamma_{\text{typ}} \sim 100$. Synchrotron emission forms another component in addition to the flat proton-induced cascade component, and its peak can be attributed to the observed peak energy. The non-linear effect on the photomeson production enhances the proton-induced cascade component compared with the case in Figure 1. As argued in Section 2.2, one sees that a hard electron distribution indeed leads to the low-energy photon index of $\alpha \sim 1$. The high-energy synchrotron spectrum of re-accelerated particles is expected to become steeper and steeper above the synchrotron peak. But, as a result of the superposition of the stochastic acceleration component and the underlying cascade component, the high-energy photon index is effectively regarded as $\beta \sim 2.5$ at $\sim 1-10$ MeV energies. As demonstrated in Figure 2, in the stochastic acceleration scenario with the electromagnetic cascade initiated by some injection at high energies, the resulting spectrum consists of an apparent broken power-law component due to the synchrotron emission from re-accelerated particles and an extra hard component from the cascade emission (including IC emission by re-accelerated particles), which is different from the previous work (Asano & Terasawa 2009) that instead obtained a simple power law with a high-energy cutoff. Such a spectrum may also be responsible for observed *Fermi* GRBs, e.g., GRB 090926B (Ackermann et al. 2011). Note that the gamma-ray luminosity in the MeV range comes from re-accelerated leptons whose energies are supplied by the plasma/MHD turbulence, so that it can be larger than a fraction of the proton luminosity that is transferred to electromagnetic components via decay of mesons and muons. The spectral break at ~ 10 keV is determined by the parameter γ_{reacc} , below which the stochastic acceleration becomes ineffective. This parameter is kept as a free one in this simulation so that the quantitative value of this low-energy break does not carry strong implications. This break's appearance is interestingly similar to the observed one reported in some of *Fermi* GRBs.

In Figure 3, we show the fate of shock-accelerated high-energy protons that are injected with a simple power law. The photomeson production efficiency is so high in this parameter set that almost all the protons are eventually depleted. Note that UHECR production without their depletion is possible at larger dissipation radii (Waxman & Bahcall 1997; Murase et al. 2008) but larger baryon loading would be required to achieve the same hadronic gamma-ray flux. One sees that high-energy mesons are mainly produced by the photomeson production, while lower-energy mesons come from

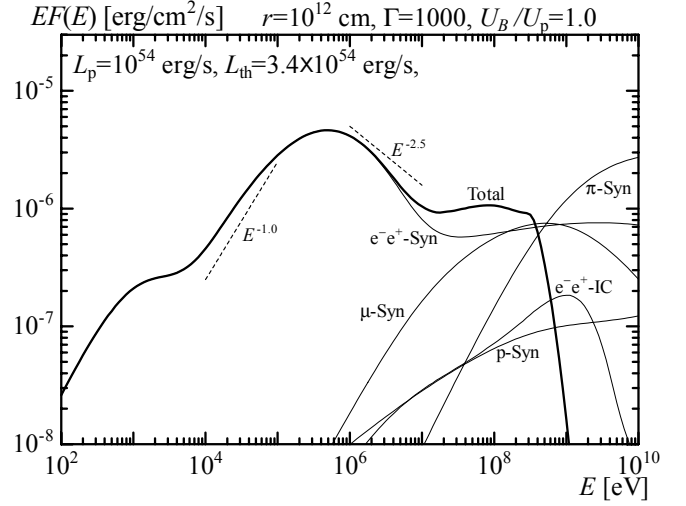


FIG. 2.— Gamma-ray spectra of proton-induced cascade emission with stochastic re-acceleration. The source redshift is assumed to be $z = 1$. Used sub-parameters (that are not critical for the result) are $l_{\text{tur}}/l = 0.17$, $\gamma_{\text{reacc}} = 10$, and $\eta = 1$. The obtained gamma-ray luminosity is $L_{\gamma} \simeq 1.2 \times 10^{53}$ erg s $^{-1}$ and the corresponding Thomson depth is $\tau_T = 1$.

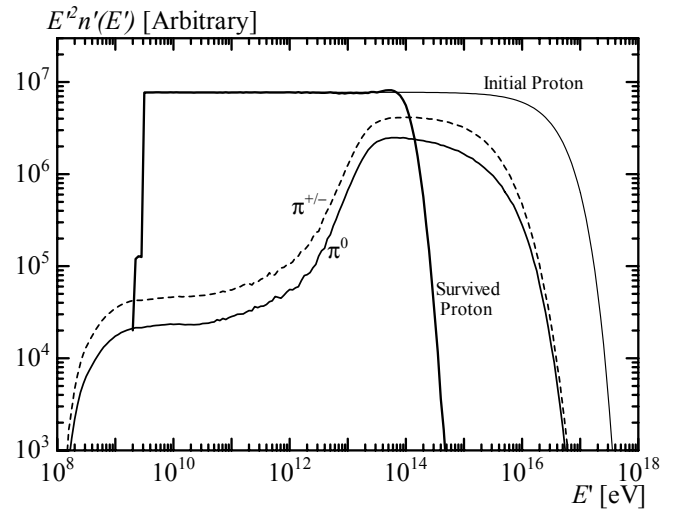


FIG. 3.— Spectra of injected and survived protons in the outflow comoving frame for the calculation in Figure 2. The resulting pion spectra are also shown.

the pp reaction, and the result is in agreement with the analytical expectation described in Section 2.1. Hence, when protons are accelerated up to sufficiently high energies, one expects that the photomeson production is typically dominant in cascaded gamma rays, though the signature of pp reactions can be seen in TeV neutrinos for sufficiently small dissipation radii. However, the pp reaction can be more important when there is no proton acceleration (e.g., Beloborodov 2010), or the nonthermal proton spectral index is steeper than 2 or proton acceleration is inefficient (Murase 2008). Such a case is demonstrated in Figure 4, where we obtain a broken power-law spectrum that can be compatible with the Band function. The value of η used here ($t_{\text{acc},p} = \eta(E_p/\Gamma eB)$) seems much larger than conventional ones that are required for UHECR acceleration, although such values have been used to interpret observed blazar spectra (e.g., Inoue & Takahara 1996).

In Figure 5, we show the result for larger emission radii,

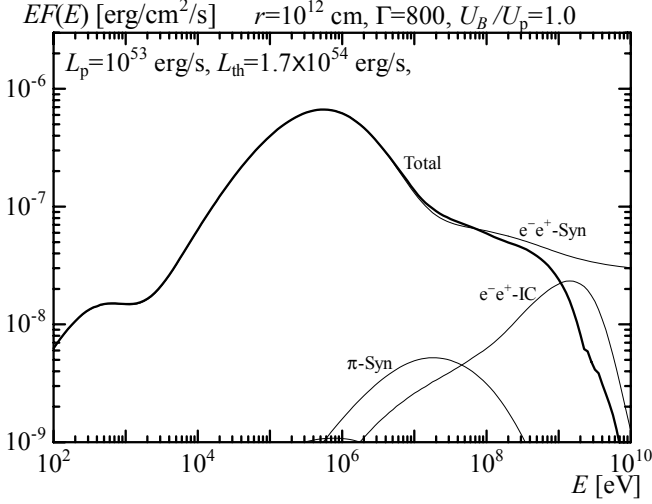


FIG. 4.— Gamma-ray spectra for the case where proton acceleration is inefficient. The source redshift is assumed to be $z = 1$. Used sub-parameters are $l_{\text{tur}}/l = 0.99$, $\gamma_{\text{reacc}} = 10$, and $\eta = 10^4$. The obtained gamma-ray luminosity is $L_\gamma \simeq 1.6 \times 10^{52}$ erg s $^{-1}$ and the corresponding Thomson depth is $\tau_T = 1$.

taking into account effects of stochastic acceleration. In this figure, a smaller magnetic field is assumed, so that IC emission from re-accelerated leptons, which is expected around 5 GeV $\gamma_{\text{typ},2}^2 (E^{\text{br}}/500 \text{ keV})$, become more prominent. The effect of the IC emission is generally non-linear, and the dependence on l_{tur} is demonstrated in Figure 6. One can see that, for larger values of l_{tur} , more particles are re-accelerated and lose their energies via the IC emission. As a result, more gamma rays are attenuated and cascaded, which enhance the extra hard component and also provide more seed photons for the photomeson prediction. The different efficiency for IC emission results in the variety of the high-energy spectral index β , which is from 2.8 to ~ 2 in Figure 6. One also sees that l_{tur} cannot be too small to have sufficiently large gamma-ray luminosities in the MeV range, but the result is not so sensitive as long as l_{tur} is large enough. Note that, the other sub-parameter, γ_{reacc} , affects the flux ratio of the broken power-law component to the power-law-like cascade component rather than l_{tur} , since more leptons can be injected to the re-acceleration process for smaller γ_{reacc} . We do not show such other cases because of the onerous calculation time involved, but our qualitative results are not much altered by these sub-parameters as long as $\gamma_{\text{reacc}} \gg \gamma_{\text{typ}}$ and l_{tur} is large enough. This is because the timescale for remaining above γ_{reacc} would be close to the diffusion timescale in energy space, $\sim \varepsilon^2/(4D_{\varepsilon\varepsilon}) = t_{\text{sta}}$. Therefore, it would not be extremely large ($\mathcal{E}_{\gamma\text{ex}}/\mathcal{E}_\gamma \gtrsim 0.01$), unless the contribution from primary electrons become relevant. Although we have considered relatively small emission radii, such a spectrum composed of an apparent broken-power law and an extra hard component is expected at larger radii too as long as high-energy injection and efficient cascades are achieved.

4. SPECIFIC IMPLICATIONS OF HADRONIC MODELS FOR HIGH-ENERGY NEUTRINO EMISSION

The purpose of our paper is to investigate the role of stochastic re-acceleration, and we specifically consider hadronic processes as high-energy injection processes. At the same time, it would be useful to discuss implications of hadronic models that can explain observed gamma rays. One

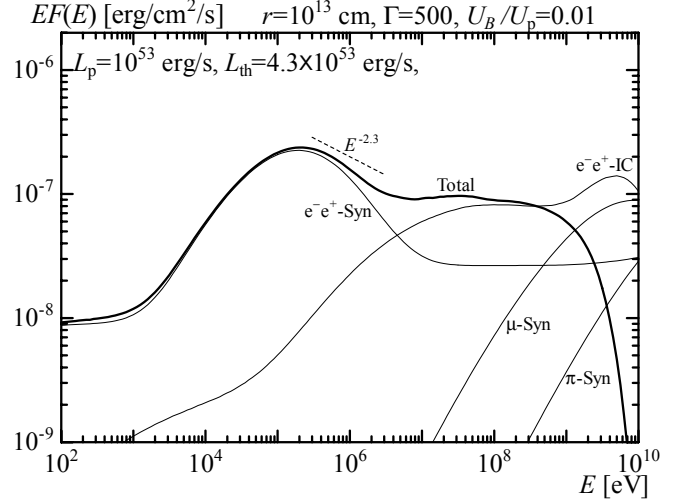


FIG. 5.— Gamma-ray spectra of proton-induced cascade emission with stochastic re-acceleration. The source redshift is assumed to be $z = 1$. Used sub-parameters are $l_{\text{tur}}/l = 0.36$, $\gamma_{\text{reacc}} = 100$, and $\eta = 1$. The obtained gamma-ray luminosity is $L_\gamma \simeq 8.6 \times 10^{51}$ erg s $^{-1}$ and the corresponding Thomson depth is $\tau_T = 0.1$.

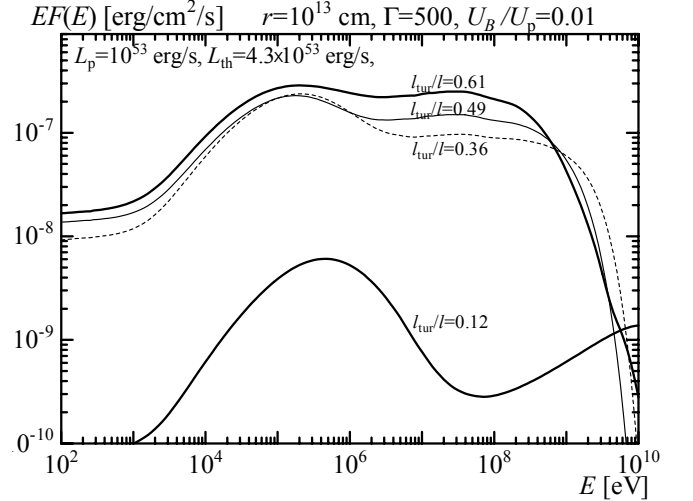


FIG. 6.— Same as Figure 5, but dependence on the sub-parameter, l_{tur} , is shown.

of the important tests of the hadronic models is the prediction of high-energy neutrinos. The high-energy neutrino emission is a generic consequence of hadronic models which explain observed gamma-ray spectra through proton-induced cascade emission rather than via proton synchrotron emission (e.g., Becker et al. 2010), whether the re-acceleration occurs or not. In the hadronic model explaining the extra hard component with the proton-induced cascade, one typically expects, $\mathcal{E}_\nu \sim \mathcal{E}_{\gamma\text{ex}}$. This relation between \mathcal{E}_ν and $\mathcal{E}_{\gamma\text{ex}}$ is not much affected by the multi-pion production effect, even though estimates of f_{mes} and the required \mathcal{E}_{CR} can be affected. However, we do not know typical values of $\mathcal{E}_{\gamma\text{ex}}$ at present, and recent analyses indicate that the GeV component is less than 10 % of the MeV one on average (e.g., Beniamini et al. 2011).

In Figure 7, we show neutrino spectra for three parameter sets shown in the previous section, when meson re-acceleration is irrelevant. For normalization, the total gamma-ray energy is set to $\mathcal{E}_\gamma^{\text{iso}} = 10^{53.5}$ erg and $z = 1$ is assumed. For

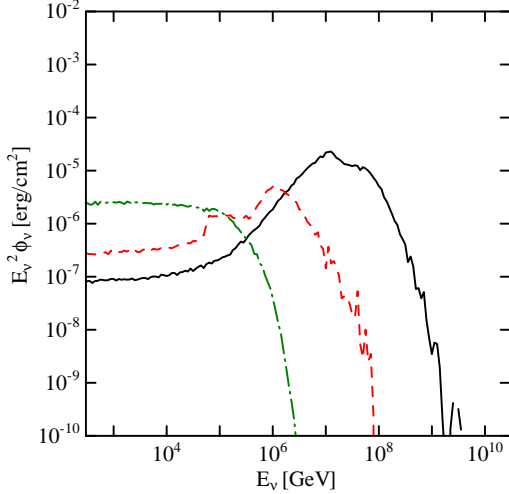


FIG. 7.— The total neutrino fluences (for all flavors) from a GRB event at $z = 1$. The dot-dashed, dashed and solid lines represent the fluences corresponding Figures 4, 3, and 5, respectively, in order of the relative importance of the pp reaction.

the thick curve where $\tau_T = 0.1$, PeV-EeV neutrinos coming from the photomeson production are mainly expected. For the dashed curve where $\tau_T = 1$, pp neutrinos become important, as in the dissipative photospheric scenario (Murase 2008; Wang & Dai 2009) and resulting in similar neutrino spectra, although our prediction comes from an independent motivation so that a larger baryon loading is typically needed to have a visible \sim GeV component. For the dot-dashed curve, only pp neutrinos are relevant because inefficient acceleration is assumed, and we do not expect \sim PeV neutrinos because the proton maximum energy is not so high. In any case, for one burst at $z \sim 1$, the expected number of muon events in IceCube is $\sim 10^{-2} - 10^{-1}$, which seems too small to detect. Hence, bright bursts with $\mathcal{E}_\nu^{\text{iso}} \gtrsim 10^{54}$ erg or nearby bursts at $z \sim 0.1$ are typically necessary (Dermer & Atoyan 2003), although they would be rare.

On the other hand, the cumulative neutrino background is of interest, since time and space coincidences are expected to be of use for analyses of GRB prompt emission. The cumulative neutrino background is calculated using the following formula,

$$\Phi_\nu = \frac{c}{4\pi H_0} \int_0^{z_{\text{max}}} dz \frac{dN_\nu((1+z)E_\nu)}{dE'_\nu} \frac{R(z)}{\sqrt{\Omega_\Lambda + \Omega_m(1+z)^3}} \quad (12)$$

where dN_ν/dE'_ν is the neutrino spectrum in the cosmological rest frame and $R(z)$ is the GRB rate. For demonstration, we use the GRB3 evolution but differences in evolution models do not make significant changes (see Murase 2007, and references therein).

An example of the cumulative neutrino background expected in the hadronic model is shown in Figure 8, using the parameters given in the caption of Figure 5. However, it is not obvious how to normalize the flux, since \mathcal{E}_γ comes from the turbulent energy rather than the cosmic-ray energy. Since $\mathcal{E}_{\gamma\text{ex}}$ is highly uncertain at present, for demonstration purposes, we introduce the differential gamma-ray energy at 100 MeV, $\tilde{\mathcal{E}}_{\gamma\text{ex}}$, and assume that it is a few % of the total gamma-ray energy. The muon neutrino flux is analytically

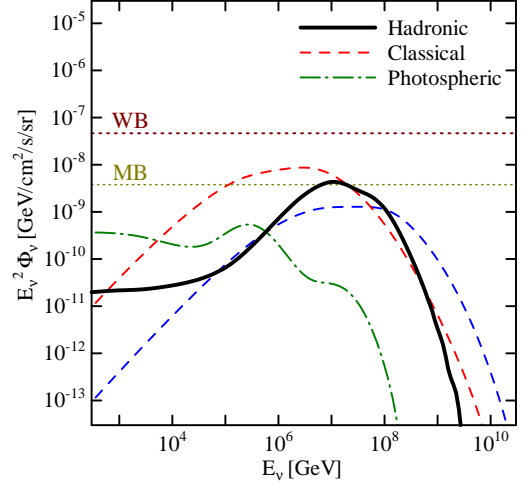


FIG. 8.— The cumulative neutrino backgrounds (for all flavors) from GRBs. Hadronic: calculated in this work for the demonstrative parameter set used in Figure 5, with normalization of $\tilde{\mathcal{E}}_{\text{HE}\gamma\text{ex}}R(0) = 10^{42}$ erg Mpc $^{-3}$ yr $^{-1}$. Classical: originally predicted by Waxman & Bahcall (1997) and numerically calculated spectra (sets A and B) are taken from Murase & Nagataki (2006a), but with normalization of $\tilde{\mathcal{E}}_{\text{HECR}}R(0) = 5 \times 10^{43}$ erg Mpc $^{-3}$ yr $^{-1}$. Photospheric: calculated in Murase (2008), but with normalization of $\xi_{\text{CR}} = 1$ and $\mathcal{E}_\gamma^{\text{iso}} = 10^{53.5}$ erg. WB: the Waxman-Bahcall bound (Waxman & Bahcall 1999) shown as landmarks. MB: the effective iron-survival bound (Murase & Beacom 2010) shown for comparison.

estimated to be

$$E_\nu^2 \Phi_\nu \sim 10^{-9} \text{ GeV cm}^{-2} \text{ s}^{-1} \tilde{\mathcal{E}}_{\text{HE}\gamma\text{ex},42} (f_z/3), \quad (13)$$

where f_z is the correction due to the redshift evolution, and the characteristic neutrino energy is generally model-dependent (cf. Figure 7). One should also keep in mind the following limitations of the result. (1) We have used the one-zone neutrino spectrum, but contributions from larger emission radii would be dominated at high energies (e.g., Murase & Nagataki 2006a). (2) The background spectrum can be affected by individual characteristics of the bursts (e.g., Becker et al. 2006), so that it would be valid for the purpose of estimating the flux level when typical parameters are chosen. In our case, if the extra hard component at $\gtrsim 10$ MeV energies is less prominent for most of the bursts, the background flux should also be less. Despite these caveats, the figure suggests that high-energy neutrino signals should be one of the important messengers of the hadronic model, and one may expect a few events per year in IceCube, provided the model assumptions are valid. Just for comparison, predictions in other scenarios are also shown in Figure 8.

Recently, the IceCube collaboration has given upper limits on the neutrino background flux (Abbasi et al. 2011), assuming the typical value of the photomeson production efficiency, $f_{p\gamma} = 0.2$. Such limits are interesting in order to test the GRB-UHECR proton hypothesis for the prompt phase (Waxman & Bahcall 1997). Generally speaking, the efficiency is model-dependent. One typically expects $\max[1, f_{p\gamma}] \sim 0.1 - 1$ for emission radii of $r \sim 10^{13} - 10^{14.5}$ cm, while $f_{p\gamma} \sim 10^{-2.5} - 10^{-1}$ for $r \sim 10^{14} - 10^{15.5}$ cm (Murase & Nagataki 2006a). Especially in the neutron escape scenario where the neutrino flux is comparable to the escaping cosmic-ray flux (e.g., Mannheim et al. 2000), the limits are already stringent for steep proton spec-

tra (Ahlers et al. 2011). However, the detection of neutrinos would typically be difficult if the observed UHECRs are mainly heavy nuclei rather than protons (Murase et al. 2008; Murase & Beacom 2010). Observations in the near future will give more stringent limits on $f_{p\gamma}$, based on the GRB-UHECR proton hypothesis. On the other hand, the hadronic model focused on in this work relies on the different motivation of explaining the observed GeV emission, where we do not have to explain UHECRs by GRBs. Since it is uncertain how common and energetic the extra hard component at $\gtrsim 10$ MeV is, it is not so obvious to derive quantitative constraints on the model. Nevertheless, although the background flux seems lower than the current limits, our result implies that future neutrino observations would be crucial for the hadronic models provided that the extra hard component commonly carries 1 – 10 % of the MeV component.

5. SUMMARY AND DISCUSSION

In this paper we studied the role of stochastic acceleration on the GRB prompt emission, in the presence of electromagnetic cascades. As an example, we employ the hadronic model to initiate cascade processes. We demonstrated that some of the current issues in the GRB prompt emission can be explained. (1) The low-energy photon index is expected to be $\alpha \sim 1$ when electrons and positrons confined in the downstream region are accelerated stochastically via turbulence, and the typical peak energy, E^{br} , is stabilized by the balance between the stochastic acceleration time and the cooling time. (2) It is possible to avoid the fast cooling problem because the charged leptons are slowly heated by turbulence. When the leptons are injected via the hadronic processes, we may not have a potential issue on injection of primary electrons in the shock acceleration mechanism. (3) An extra hard component, $EF(E) \propto E^{0-0.5}$, which has often been observed above 1 – 100 MeV, can be explained by cascade emission, such as in proton-induced cascades. The existence of the extra component is an important feature of the cascade initiated by high-energy injection well above MeV energies.

Although we have considered one-zone cases, dissipation will occur at various radii, which can affect the high-energy spectrum. As shown in appendix B, in slow heating scenarios via stochastic acceleration, the high-energy photon spectrum can be harder than in the one-zone case because of the superposition of one-zone slow-heating spectra. As a result, the broadband spectral shape can be a broken power law up to \sim GeV energies. Such multi-zone effects are even more important above $\gtrsim 0.1$ GeV. Smaller $\gamma\gamma$ opacities at larger radii generally smear out the $\gamma\gamma$ pair-creation cutoff (Aoi et al. 2010). Note that, in our calculation method (where spectra are obtained via iteration), the radiative transfer effect, which leads to $(1 - \exp(-\tau_{\gamma\gamma}))/\tau_{\gamma\gamma}$ rather than the exponential cutoff, is not included. Also, time-dependent and geometrical effects introduce additional complications, and the pair-creation break can be higher (Granot et al. 2008). Hence, we expect that the extra component extends to higher energies, although details are beyond the scope of this work.

One of the observational properties found by *Fermi* is the delayed onset at GeV energies. It is not so obvious how to explain this in our model. However, there are several reasons that may lead to broader pulses at high energies. Especially, multi-zone effects seem important. As expected from the above, the cascade component as well as the slow heated component would be superposed by dissipation at various radii. Also, gamma rays from outer radii would be more transpar-

ent, which could make a dominant contribution at GeV-TeV energies. In addition, in the hadronic models, neutron beams from the inner radius make further gamma rays via neutron decay and photomeson production with low-energy photons produced by dissipation at the outer radius. Leptons may also up-scatter the MeV emission from inner radii via the external IC process. In addition, in our model, emissions on timescales longer than t_{tur} and t_{dyn} are expected. Even after the dynamical time, the residual energy of electrons would be released by the external IC process and synchrotron radiation in some residual magnetic field. In the hadronic models, further hadronic reactions may also happen as the escaping cosmic rays diffuse in the residual magnetic field (although they are adiabatically cooled). Hence, future refinements based on multi-zone calculations seems necessary.

All hadronic models have typically several caveats or open issues. They often lead to the requirement of a high baryon loading, which may be problematic, although this is motivated mainly by the GRB-UHECR hypothesis. Another potential issue is the radiative efficiency. In our cases, we typically obtain $L_{\gamma}/L_{\text{th}} \sim 0.1$, although the apparent radiative efficiency can be higher due to lower γ_{reacc} , release of the cosmic rays, residual emission and subsequent internal collisions. Despite these concerns, there are interesting features. Importantly, the hadronic model seems testable by upcoming multi-messenger observations. The high-energy neutrino signal is one of the most important signatures, since the neutrino luminosity is expected to be comparable to the extra hard component. If this extra component is ubiquitous and it carries $\sim 1 - 10$ % of the total gamma-ray energy, IceCube would detect this signal in multi-year observations. It is also important to check whether the extra hard component is common among all GRBs. As of now, its detectability with *Fermi* is limited and the current analyses suggest that the GeV emission has less than ~ 10 % of the MeV emission. Therefore, in order to unravel the properties of the high-energy emission, deeper observations via detections with Cherenkov detectors such as MAGIC and VERITAS should be important, even though detections from distant GRBs become difficult due to the attenuation by the extragalactic background light. Although very-high-energy photons from GRBs have not been firmly detected so far, the future CTA (CTA Consortium 2010) and HAWC are anticipated to change this situation.

We note that, although we have focused on the hadronic model as an example of high-energy injection, our results can be applied to other models, e.g., such as magnetic dissipation. In the slow heating scenario resulting from stochastic acceleration, it seems common to have hard low-energy photon indices, $\alpha \sim 1$ and $\beta > 2$. This feature itself would not be changed by details of the high-energy injection, as long as slow heating can operate and the MeV peak comes from balance between heating and cooling. Hence, as for the origin of stochastically accelerated particles, one may think of other high-energy injection processes and subsequent cascades. If magnetic dissipation such as reconnection accelerates electrons up to very high energies and subsequent cascades are developed, similar spectra would be obtained.

K.M. is greatly thankful to Tatsumi Koi for technical support to use Geant 4, and a part of calculations was carried out on Altix3700 BX2 at YITP in Kyoto University. We thank Soebur Razzaque and Kenji Toma for useful suggestions and discussions. K.M. acknowledges financial support by a Grant-

in-Aid from JSPS, from CCAPP and from PSU. K.M. also thanks the hospitality of TIT and PSU, during a part of this project. This study is partially supported by Grants-in-Aid for Scientific Research No. 22740117 from the Ministry of Edu-

cation, Culture, Sports, Science and Technology (MEXT) of Japan (K.A.). P.M. acknowledges partial support from NASA NNX08AL40G and NSF PHY-0757155.

APPENDIX

STOCHASTIC RE-ACCELERATION OF MESONS AND MUONS

Here, we consider the possible effect of re-accelerated mesons on high-energy neutrino spectra. First, for $E_\nu^{\text{br}} < E_\nu^s$, the classical neutrino spectrum produced by shock accelerated protons via the photomeson production is written as (Waxman & Bahcall 1999; Rachen & Mészáros 1998; Waxman 2011; Murase 2007)

$$E_\nu^2 \phi_\nu \propto \begin{cases} (E_\nu/E_\nu^{\text{br}})^{\beta-1} & (E_\nu \leq E_\nu^{\text{br}}) \\ (E_\nu/E_\nu^{\text{br}})^{\alpha-1} & (E_\nu^{\text{br}} < E_\nu \leq E_\nu^s) \\ (E_\nu^s/E_\nu^{\text{br}})^{\alpha-1} (E_\nu/E_\nu^s)^{\alpha-3} & (E_\nu^s < E_\nu) \end{cases} \quad (\text{A1})$$

Here E_ν^{br} is the low-energy break coming from $E_\nu^{\text{br}} \approx 0.05 E_p^{\text{br}}$ or the characteristic energy where $f_{p\gamma}(20E_\nu) = 1$ (Asano 2005; Murase & Nagataki 2006a). Also, we have only assumed the pion synchrotron loss as the important cooling process, and $E_\nu^s \approx 0.25 E_\pi^s$ is the high-energy break coming from the pion synchrotron loss, though other processes such as adiabatic cooling could also be relevant. From $t_{\pi, \text{syn}} = t_\pi \equiv \gamma_\pi \tau_\pi$ (where τ_π is the lifetime of charged pions), the high-energy break energy of pions is estimated to be

$$E_\pi^s \approx \sqrt{\frac{6\pi(m_\pi c^2)^5}{\sigma_T m_e^2 c^5 B^2 \tau_\pi}} \simeq 190 \text{ PeV } \epsilon_{B,-1} r_{13} L_{\text{th},53.5}^{-1/2} \Gamma_{2.7}^2. \quad (\text{A2})$$

Note that one can make similar estimates for other particles such as kaon and muons, changing proper mass and lifetime.

If there is re-acceleration by turbulence, $t_{\pi, \text{sta}} = t_{\pi, \text{syn}}$ gives the maximum energy of accelerated pions unless the energy fraction carried by mesons exceeds ϵ_π , similarly to the case of electrons. When one uses equation (9), the typical energy of pions is estimated to be

$$E_\pi^{\text{typ}} \approx \left[\frac{6\pi m_\pi^4 c^4 (eB)^{2-q}}{\sigma_T m_e^2 B^2 l_{\text{tur}}^{q-1} \eta_{\text{sta}}} \right]^{\frac{1}{3-q}}. \quad (\text{A3})$$

The situation depends on details of the plasma/MHD turbulence at relevant scales. As numerical examples, we have $E_\pi^{\text{typ}} \simeq 120 \text{ PeV } \epsilon_{B,-1}^{-3/4} r_{13}^{3/2} l_{\text{tur},10}^{-2/3} L_{\text{th},53.5}^{-3/4} \Gamma_{2.7}^{5/2} \eta_{\text{sta}}^{5/6}$ for $q = 1.8$, and $E_\pi^{\text{typ}} \simeq 880 \text{ PeV } \epsilon_{B,-1}^{-1/2} r_{13} l_{\text{tur},10}^{-1/3} L_{\text{th},53.5}^{-1/2} \Gamma_{2.7}^2 \eta_{\text{sta}}^{2/3}$ for $q = 1.5$. However, the re-acceleration of charged mesons is possible only when particles are injected to the re-acceleration process before their decay. The critical energy is determined by $t_\pi = t_{\pi, \text{sta}}$, and we find

$$E_\pi^{\text{cr}} \approx \left(\frac{\tau_\pi (eB)^{2-q} l_{\text{tur}}^{1-q}}{m_\pi c \eta_{\text{sta}}} \right)^{\frac{1}{1-q}}. \quad (\text{A4})$$

For $1 < q < 2$, we expect two cases, $E_\pi^{\text{cr}} < E_\pi^s < E_\pi^{\text{typ}}$ and $E_\pi^{\text{typ}} < E_\pi^s < E_\pi^{\text{cr}}$, and re-acceleration of mesons is relevant only in the former case at energies above E_π^{cr} . For $q < 1$, two cases, $E_\pi^s < E_\pi^{\text{typ}} < E_\pi^{\text{cr}}$ and $E_\pi^{\text{cr}} < E_\pi^{\text{typ}} < E_\pi^s$, are possible, and mesons with energies below E_π^{cr} are re-accelerated in the former case. Usually such re-acceleration will not be important at large dissipation radii especially above the photospheric radius, since time scales such as t_{sta} , t_{cool} and t_{dyn} become longer for larger radii whereas t_π is unaffected. If the meson re-acceleration happens, mesons are re-distributed so that the resulting meson spectrum will be altered. As long as particle escape is irrelevant, the neutrino spectrum can be hard, and one may expect

$$E_\nu^2 \phi_\nu \propto E^{3-q} (E_\nu \leq E_\nu^{\text{typ}}). \quad (\text{A5})$$

The typical neutrino energy can be very high energies of $\sim 100 \text{ PeV}$, so that detectability of such very high-energy neutrinos may be enhanced by re-acceleration.

SUPERPOSITION OF SLOW HEATING SPECTRA

In the slow heating scenario with stochastic acceleration, whether the origin of relativistic electrons (and positrons) is leptonic or hadronic, one may expect a synchrotron component with a hard spectrum,

$$EF(E) \propto E^{2-\alpha} (E \leq E^{\text{br}}), \quad (\text{B1})$$

where $\alpha \sim q/2$ if the MHD turbulence is responsible for stochastic acceleration. Above E^{br} , the spectrum would typically have a cutoff feature or significant steepening ($\beta \gg 2$).

So far, we have assumed the one-zone case, where dissipation occurs at the specific radius, r . But, realistically, dissipation continues at further radii, and we discuss its effect on the high-energy spectrum. For simplicity, let us here assume that $L_\gamma, L_B \propto L_{\text{diss}} \propto r^{-s}$ ($s > 0$). For a given Γ , assuming $l_{\text{tur}} \propto l \propto r$, one obtains

$$t_{\text{sta}} \propto B^{q-2} \gamma^{2-q} l_{\text{tur}}^{q-1} \propto r^{q-1+(q/2-1)(s+2)} \gamma^{2-q}. \quad (\text{B2})$$

On the other hand, the (synchrotron/IC) cooling timescale has

$$t_{\text{cool}} \propto r^2 L_{\text{diss}}^{-1} \gamma^{-1} \propto r^{(s+2)} \gamma^{-1}. \quad (\text{B3})$$

Then, for the synchrotron break energy, we have

$$E^{\text{br}} \propto \gamma_{\text{typ}}^2 B \propto r^{(s+2)/(3-q)-(s+1)}. \quad (\text{B4})$$

As a result, if the one-zone high-energy photon spectrum above E^b is steep enough, the multi-zone high-energy photon spectrum may have a harder one,

$$EF(E) \propto E^{-\frac{s(3-q)}{(s+2)-(s+1)(3-q)}}. \quad (\text{B5})$$

Especially if $q \sim 2$, one has $EF(E) \propto E^{-s}$ which may be responsible for the high-energy index. In this case, higher-energy gamma rays are emitted mainly from larger radii, so that those timescales can in principle be longer. Note that the above discussion can be applied to not only the shock dissipation models but also the magnetic dissipation models, and a broken power-law spectrum can be expected in either case.

REFERENCES

- Abbasi, R., et al. 2011, *Phys. Rev. Lett.*, 106, 141101
 Abdo, A. A., et al. 2009a, *Science*, 323, 1688
 Abdo, A. A., et al. 2009b, 706, L138
 Abdo, A. A., et al. 2009c, *ApJ*, 707, 580
 Abdo, A. A., et al. 2010, *ApJ*, 712, 558
 Ackermann, M., et al. 2010, *ApJ*, 712, 558
 Ackermann, M., et al. 2011, *ApJ*, 729, 114
 Ahlers, M., Gonzalez-Garcia, M. C., & Halzen, F. 2011, arXiv:1103.3421
 Agostinelli, S., et al. 2003, *Nucl. Instrum. Methods Phys. Res., Sect. A*, 506, 250
 Aoi, J., Murase, K., Takahashi, K., Ioka, K., & Nagataki, S. 2010, *ApJ*, 722, 440
 Asano, K. 2005, *ApJ*, 623, 967
 Asano, K., & Inoue, S. 2007, *ApJ*, 655, 762
 Asano, K., & Nagataki, S. 2006, *ApJ*, 640, L9
 Asano, K., & Takahara, T. 2003, *PASJ*, 55, 433
 Asano, K., & Terasawa, T. 2009, *ApJ*, 705, 1714
 Asano, K., Inoue, S., & Mészáros, P. 2009a, *ApJ*, 699, 953
 Asano, K., Guiriec, S., & Mészáros, P. 2009b, *ApJ*, 705, L191
 Baerwald, P., Hümmer, S., & Winter, W. 2011, *Phys. Rev. D*, 83, 067303
 Baring, M. G. 2006, *ApJ*, 650, 1004
 Becker, J. K., Stamatikos, M., Halzen, F., Rhode, & W. 2006, *Astropart. Phys.*, 25, 118
 Becker, J. K., Halzen, F., Murchadha, A. O., & Olivo, M. 2010, *ApJ*, 721, 1891
 Bednarz, J., & Ostrowski, M. 1996, *MNRAS*, 283, 447
 Beloborodov, A. M. 2000, *ApJ*, 539, L25
 Beloborodov, A. M. 2010, *MNRAS*, 407, 1033
 Beniamini, P., Guetta, D., Nakar, E., & Piran, T. 2011, arXiv:1103.0745
 Blumenthal, G. R., & Gould, R. J. 1970, *Rev. Mod. Phys.*, 42, 237
 Brunetti, G., & Lazarian, A. 2007, *MNRAS*, 378, 245
 Bykov, A. M., & Mészáros, P. *ApJ*, 461, L37
 Chang, P., Spitkovsky, A., & Arons, J. 2008, *ApJ*, 674, 378
 Chodorowski, M. J., A. Zdziarski, A. A., & Sikora, S. R. 1992 *ApJ*, 400, 181
 Corsi, A., Guetta, D., & Piro, L. 2010, *ApJ*, 499, L31
 CTA Consortium 2010, arXiv:1008.3703
 Daigne, F., Bosnjak, Z., & Dubus, G. 2011, *A&A*, 526, 110
 Derishev, E. V., Kocharovsky, V. V., & Kocharovsky, VI. V. 2001, *A&A*, 372, 1071
 Dermer, C. D., & Atayan, A. 2003, *Phys. Rev. Lett.*, 91, 071102
 Dermer, C. D., & Atayan, A. 2006, *New. J. Phys.*, 8, 122
 Dermer, C. D., Miller, J. A., & Li, H. 1996, *ApJ*, 456, 106
 Eichler, D., & Waxman, E. 2005, *ApJ*, 627, 861
 Ghisellini, G., & Celotti, A. 1999, *ApJ*, 511, L93
 Ghisellini, G., et al. 2010, *MNRAS*, 403, 926
 Granot, J. 2010, arXiv:1003.2452
 Granot, J., Cohen-Tanugi, J., do Couto e Silva, E. 2008, *ApJ*, 677, 92
 Gupta, N., & Zhang, B. 2008, *MNRAS*, 384, L11
 He, H. N., et al. 2011, *ApJ*, 733, 22
 Hurley, K., et al. 1994, *Nature*, 372, 652
 Ioka, K. 2010, *Prog. Theo. Phys.*, 124, 667
 Ioka, K., Toma, K., Yamazaki, R., & Nakamura, T. 2006, *A&A*, 458, 7
 Ioka, K., Murase, K., Toma, K., Nagataki, S., & Nakamura, T. 2007, *ApJ*, 670, L77
 Inoue, S., & Takahara, F. 1996, *ApJ*, 463, 555
 Inoue, T., Asano, K., & Ioka, K. 2011, *ApJ*, 734, 77
 Kumar, P., & Barniol Duran, R. 2010, *MNRAS*, 409, 226
 Lithwick, Y., & Sari, R. 2001, *ApJ*, 555, 540
 Liu, S., Melia, F., Petrosian, V., & Fatuzzo, M. 2006, *ApJ*, 647, 1099
 Lyutikov, M. 2006, *New. J. of Phys.*, 8, 119
 Mannheim, K., Protheroe, R. J., & Rachen, J. P. 2000, *Phys. Rev. D* 63, 023003
 McKinney, J. C., & Uzdensky, D. A. 2011, arXiv:1011.1904
 Medvedev, M. V. 2000, *ApJ*, 540, 704
 Medvedev, M. V., & Spitkovsky, A. 2009, *ApJ*, 700, 956
 Mészáros, P. 2006, *Rep. Prog. Phys.*, 69, 2259
 Mészáros, & P., Rees, M. J. 2000, *ApJ*, 530, 292
 Miller, J. A., & Ramaty, R. 1989, *ApJ*, 344, 973
 Mizuno, Y., et al. 2011, *ApJ*, 726, 62
 Murase, K. 2007, *Phys. Rev. D*, 76, 123001
 Murase, K. 2008, *Phys. Rev. D*, 78, 101302(R)
 Murase, K. 2009, *Phys. Rev. Lett.*, 103, 081102
 Murase, K., & Beacom, J. F. 2010, *Phys. Rev. D*, 81, 123001
 Murase, K., & Nagataki, S. 2006a, *Phys. Rev. D*, 73, 063002
 Murase, K., & Nagataki, S. 2006b, *Phys. Rev. Lett.*, 97, 051101
 Murase, K., Ioka, K., Nagataki, S., & Nakamura, T. 2008, *Phys. Rev. D*, 78, 023005
 Pe'er, A., Mészáros, P., & Rees, M. J. 2006, *ApJ*, 642, 995
 Pe'er, A., & Zhang, B. 2006, *ApJ*, 653, 454
 Pe'er, A., et al. 2011, arXiv:1007.2228
 Petrosian, V., & Liu, S. 2004, *ApJ*, 610, 550
 Rachen, J. P., & Mészáros, P. 1998, *Phys. Rev. D*, 58, 123005
 Razzaque, S. 2011, *ApJ*, 724, L109
 Razzaque, S., Dermer, C. D., Finke, J. D. 2010, *OAJ*, 3, 150
 Rees, M. J., & Mészáros, P. 1994, *ApJ*, 430, L93
 Sironi, L., & Spitkovsky, A. 2011, 726, 75
 Spruit, H. C., Daigne, F., & Drenkhahn, G. 2001, *A&A*, 369, 694
 Svensson, R. 1987, *MNRAS*, 227, 403
 Thompson, C. 1994, *MNRAS*, 270, 480
 Totani, T. 1998, *ApJ*, 509, L81
 Toma, K., Wu, X. F., & Mészáros, P. 2011, arXiv:1002.2634
 Vietri, M. 1995, *ApJ*, 453, 883
 Vietri, M. 1997, *Phys. Rev. Lett.*, 78, 4328
 Vurm, I., Beloborodov, A. M., & Poutanen, J. 2011, arXiv:1104.0394
 Vurm, I., & Poutanen, J. 2009, *ApJ*, 698, 293
 Wang, X. Y., & Dai, Z. G. 2009, *ApJ*, 691, L67
 Wang, X. Y., Li, Z., Dai, Z. G., & Mészáros, P. 2009, *ApJ*, 698, L98
 Waxman, E. 1995, *Phys. Rev. Lett.*, 75, 386
 Waxman, E. 2010, arXiv:1010.5007
 Waxman, E. 2011, arXiv:1101.1155
 Waxman, E., & Bahcall, J. 1997, *Phys. Rev. Lett.*, 78, 2292
 Waxman, E., & Bahcall, J. 1997, *Phys. Rev. D*, 59, 023002
 Yonetoku, D., et al. 2004, *ApJ*, 609, 935
 Zhang, B. 2007, *ChJAA*, 7, 1
 Zhang, B., & Yan, H. 2011, *ApJ*, 726, 90
 Zhang, B., et al. 2007, *ApJ*, 655, 989
 Zhang, W., MacFayden, A., & Wang, P. 2009, *ApJ*, 692, L40